Monthly Notices of the ROYAL ASTRONOMICAL SOCIETY

MNRAS **522,** 2181–2187 (2023) https://doi.org/10.1093/mnras/stad1113
Advance Access publication 2023 April 18

WD J004917.14−252556.81: the most massive pulsating white dwarf

Mukremin Kilic [1]★ Alejandro H. Córsico,[2,3] Adam G. Moss,[1] Gracyn Jewett,[1]
Francisco C. De Gerónimo[4,5] and Leandro G. Althaus[2,3]

[1]*Homer L. Dodge Department of Physics and Astronomy, University of Oklahoma, 440 W. Brooks Str., Norman, OK 73019, USA*
[2]*Grupo de Evolución Estelar y Pulsaciones, Facultad de Ciencias Astronómicas y Geofísicas, Universidad Nacional de La Plata, Paseo del Bosque s/n, 1900 La Plata, Argentina*
[3]*IALP - CONICET, 1900 La Plata, Argentina*
[4]*Instituto de Astrofísica, Pontificia Universidad Católica de Chile, Av. Vicuña Mackenna 4860, 7820436 Macul, Santiago, Chile*
[5]*Millennium Institute of Astrophysics, Nuncio Monseñor Sotero Sanz 100, Of. 104, Providencia, 4860 Santiago, Chile*

Accepted 2023 April 6. Received 2023 April 4; in original form 2023 February 16

ABSTRACT

We present Apache Point Observatory (APO) and Gemini time-series photometry of WD J004917.14−252556.81, an ultramassive DA white dwarf with $T_{\rm eff}$ = 13 020 K and log g = 9.34. We detect variability at two significant frequencies, making J0049−2525 the most massive pulsating white dwarf currently known with $M_\star = 1.31\,{\rm M}_\odot$ (for a CO core) or $1.26\,{\rm M}_\odot$ (for an ONe core). J0049−2525 does not display any of the signatures of binary mergers, there is no evidence of magnetism, large tangential velocity, or rapid rotation. Hence, it likely formed through single star evolution and is likely to have an ONe core. Evolutionary models indicate that its interior is $\gtrsim$99 per cent crystallized. Asteroseismology offers an unprecedented opportunity to probe its interior structure. However, the relatively few pulsation modes detected limit our ability to obtain robust seismic solutions. Instead, we provide several representative solutions that could explain the observed properties of this star. Extensive follow-up time-series photometry of this unique target has the potential to discover a significant number of additional pulsation modes that would help overcome the degeneracies in the asteroseismic fits, and enable us to probe the interior of an $\approx 1.3\,{\rm M}_\odot$ crystallized white dwarf.

Key words: stars: evolution – stars: oscillations – stars: variables: general – white dwarfs.

1 INTRODUCTION

The majority of stars that evolve in isolation end up as CO core white dwarfs (Fontaine, Brassard & Bergeron 2001). Mass transfer in a binary can cut the evolution of a star short, leading up to the formation of low-mass white dwarfs with He cores and masses below about $0.45\,{\rm M}_\odot$. On the opposite end of the mass spectrum, off-centre carbon ignition in a degenerate CO core with $M \geq 1.06\,{\rm M}_\odot$ should lead to the formation of ONe core white dwarfs (Murai et al. 1968). However, binary mergers may also form CO core white dwarfs in the same mass range (e.g. Althaus et al. 2021, but see Schwab 2021). Observationally, it is nearly impossible to constrain the core composition of a white dwarf.

Kepler, Koester & Ourique (2016) reported the discovery of a white dwarf with an atmosphere dominated by O, Ne, and Mg with abundance ratios of O/Ne = 25 and O/Mg = 55. The lack of any H or He lines in the spectrum of this star, along with its ONeMg atmosphere, make it an excellent candidate for an ONe core white dwarf. Asteroseismology is the only method that can probe the interior structure and core composition (Fontaine & Brassard 2008; Winget & Kepler 2008; Giammichele et al. 2018; Córsico et al. 2019a), though with few exceptions, the majority of the pulsating white dwarfs known have $M < 1.06\,{\rm M}_\odot$, and therefore are expected to have CO cores.

There are three pulsating white dwarfs with mass estimates above $M_\star > 1.1\,{\rm M}_\odot$ as reported in the literature. BPM 37093 (Kanaan et al. 1992) is a $T_{\rm eff} = 11\,620 \pm 189$ K and $M_\star = 1.13 \pm 0.14\,{\rm M}_\odot$ (Bédard, Bergeron & Fontaine 2017) DAV white dwarf with pulsation periods of 512–635 s (Metcalfe, Montgomery & Kanaan 2004). GD 518 shows pulsations with periods of 425–595 s (Hermes et al. 2013), and has $T_{\rm eff} = 12\,030 \pm 210$ K and $M_\star = 1.23 \pm 0.03\,{\rm M}_\odot$ based on the 1D atmosphere models and a CO core (Gianninas, Bergeron & Ruiz 2011). However, a recent analysis based on *Gaia* parallax indicates a lower mass, with the best-fitting parameters of $T_{\rm eff} = 11\,422 \pm 106$ K and $M_\star = 1.114 \pm 0.006\,{\rm M}_\odot$ (Kilic et al. 2020). SDSS J084021.23+522217.4 is another DAV with pulsations periods of 173–797 s (Curd et al. 2017) and has a spectroscopic mass estimate above $1.1\,{\rm M}_\odot$, but the photometric method and *Gaia* parallax indicate a mass below $1\,{\rm M}_\odot$ in the Montreal White Dwarf Database (Dufour et al. 2017).

Rowan et al. (2019) and Vincent, Bergeron & Lafrenière (2020) identified three additional pulsating white dwarf candidates with a mass $\geq 1.05\,{\rm M}_\odot$. However, none of these three objects have follow-up spectroscopy available in the literature, and they all show variations at a single dominant period of 330, 357, and 809 s, respectively. Rapidly rotating white dwarfs are known to show photometric variations at similar periods (Pshirkov et al. 2020; Caiazzo et al. 2021), and they may impersonate ZZ Ceti white dwarfs (Kilic et al. 2021b). Hence, further spectroscopy and time-series photometry are necessary to confirm that these three targets are indeed DA white dwarfs with multiperiodic photometric variations due to pulsations.

★ E-mail: kilic@ou.edu

Table 1. Physical parameters of J004917.14−252556.81.

Parameter	Value
Spectral Type	DA
$T_{\rm eff}$ (K)	13020 ± 460
$\log g$	9.341 ± 0.036
Distance (pc)	$99.7^{+2.9}_{-2.7}$
Mass, ONe core ($M_\odot$)	1.263 ± 0.011
Cooling age, ONe core (Gyr)	1.94 ± 0.08
Mass, CO core ($M_\odot$)	1.312 ± 0.010
Cooling age, CO core (Gyr)	1.72 ± 0.09

Recently, Kilic et al. (2021a) presented an analysis of the ultramassive ($M_\star \geq 1.3\,M_\odot$) white dwarf candidates in the Montreal White Dwarf Database 100 pc sample, and identified 25 white dwarfs with masses up to 1.35 $M_\odot$, assuming CO core composition. Kilic et al. (2023) presented spectroscopic and photometric follow-up observations of this sample to constrain the merger fraction among this population. In this process, they also identified an exciting ZZ Ceti candidate. Table 1 presents the physical parameters of WD J004917.14−252556.81, which is a DA white dwarf with $T_{\rm eff} = 13020 \pm 460$ K and $\log g = 9.341 \pm 0.036$. These parameters make it by far the best ZZ Ceti candidate in the 100 pc sample of ultramassive white dwarfs. However, J0049−2525 has no prior time-series photometry available.

Here, we present APO and Gemini time-series photometry of J0049−2525. We detect multiperiodic photometric variability, making J0049−2525 the most massive pulsating white dwarf currently known. We present the details of our observations in Section 2, the pulsation spectrum of J0049−2525 in Section 3, and results from our representative asteroseismic models in Section 4. We conclude in Section 5.

2 HIGH-CADENCE PHOTOMETRY

We acquired high speed photometry of J0049−2525 on UT 2022 December 22 using the APO 3.5 m telescope with the *Agile* frame transfer camera (Mukadam et al. 2011) and the BG40 filter. We obtained back-to-back exposures of 30 s over 2 h. We binned the CCD by 2 × 2, which resulted in a plate scale of 0.258 arcsec pixel^{-1}. Given the southern declination of this target, our observations were obtained under 2.5 arcsec seeing and an airmass of 2. In addition, due to the 2.2 arcmin field of view of *Agile*, there was only one reference star available. Even with these setbacks, we detected significant photometric variations in J0049−2525, which prompted us to ask for the Director's Discretionary Time on Gemini South.

We obtained Gemini GMOS time-series photometry of J0049−2525 on UT 2022 December 26 and 27 as part of the programme GS-2022B-DD-107. We obtained 121 and 215 × 7 s back-to-back exposures on December 26 and 27, respectively. We used the SDSS-*g* filter, and binned the chip by 4 × 4. This resulted in a plate scale of 0.32 arcsec pixel^{-1} and a 15.7 s overhead, resulting in a cadence of 22.7 s. We used four reference stars brighter than J0049−2525 for relative photometry.

We obtained additional APO photometry of J0049−2525 on UT 2023 January 8 using the same setup as above. We obtained 360 × 15 s back to back exposures with *Agile*.

3 PULSATIONS IN J0049−2525

Fig. 1 shows the APO light curves of J0049−2525 from UT 2022 December 22 and 2023 January 8 and their Fourier transforms (bottom panels). The black lines show the original spectrum (shown in red) pre-whitened by the dominant peak. The data from the first night shows two frequencies, near 390 and 410 cycles per day, above the 4⟨A⟩ level, where ⟨A⟩ is the average amplitude in the Fourier transform. The dominant frequency has ≈30 mmag amplitude, and is detected at high significance. However, the pre-whitening of the Fourier transform by the dominant frequency lowers the amplitude of the secondary peak to below the 4⟨A⟩ level.

Interestingly, these two frequencies seem to be persistent in the second night of APO data (see the right panels in Fig. 1). Here the dominant frequency has actually switched. The second frequency near 410 cycles per day is detected above the 5⟨A⟩ level with an amplitude of 35 mmag, while the first frequency near 390 cycles per day is present at below the 4⟨A⟩ level. Since both frequencies are persistent on two nights of observations from APO, and both show amplitude variations, these data clearly indicate that J0049−2525

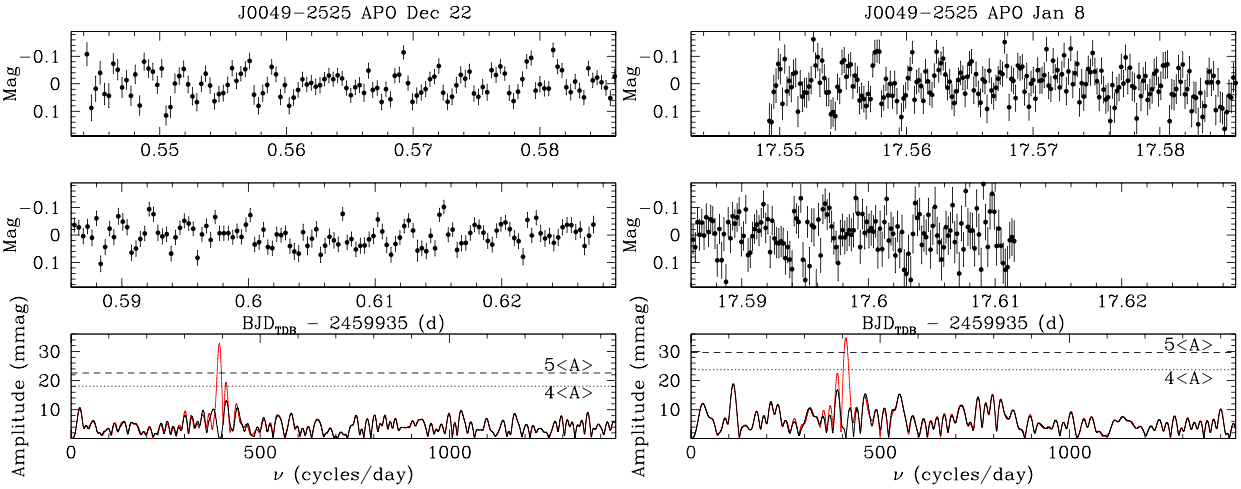

Figure 1. APO time-series photometry of J0049−2525 on two separate nights (top panels). The bottom panels show the Fourier transform of each light curve before (red) and after (black) pre-whitening of the dominant frequency. The dotted and dashed lines mark the 4 and 5⟨A⟩ level, where ⟨A⟩ is the average amplitude in the Fourier transform.

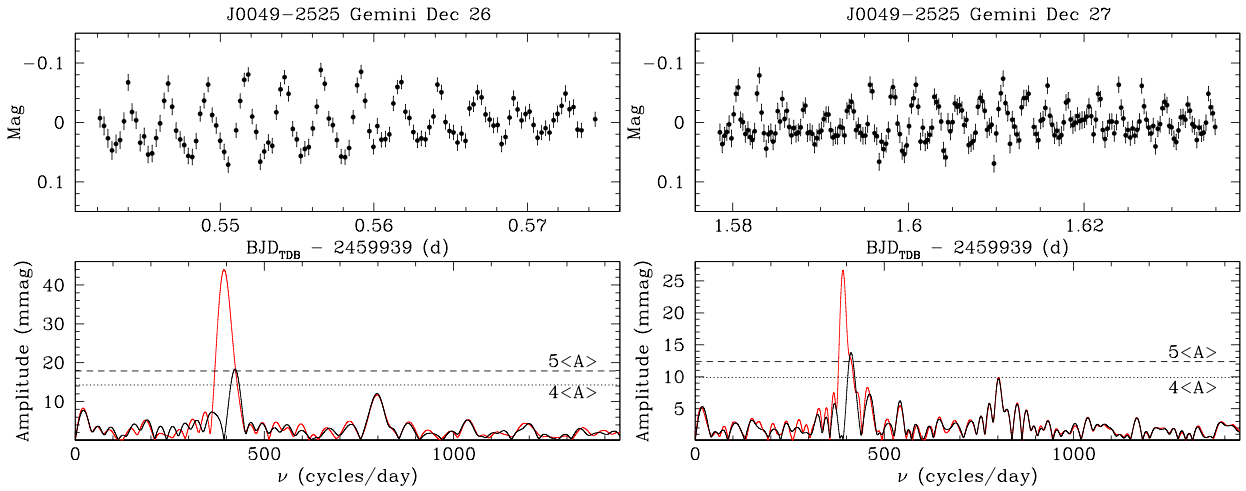

Figure 2. Gemini time-series photometry of J0049−2525 obtained over two consecutive nights. The panels and labels are the same as in Fig. 1. The observations span 47 (left) and 81 min (right), respectively.

Table 2. Multimode frequency solutions based on the APO data.

Date	ID	Method	Frequency (cycles d^{-1})	Period (s)	Amplitude (mmag)
2022 Dec 22	F1	LSQ	391.64 ± 0.72	220.61 ± 0.40	30.3 ± 3.3
2023 Jan 8	F2	LSQ	409.14 ± 1.19	211.18 ± 0.61	34.6 ± 4.7
2022 Dec 22	F1	MC	$391.94^{+0.75}_{-0.90}$	$220.44^{+0.50}_{-0.42}$	$32.2^{+2.8}_{-3.3}$
2023 Jan 8	F2	MC	$409.13^{+1.29}_{-1.23}$	$211.18^{+0.63}_{-0.66}$	$35.0^{+4.2}_{-4.3}$

shows multiperiodic variability due to pulsations. Further support comes from the Gemini data.

Fig. 2 shows the Gemini light curves of J0049−2525 from UT 2022 December 26 and 27 along with their Fourier transforms. Even though Gemini observations have a shorter baseline, the data quality is significantly better. These light curves show peak-to-peak variations that vary over time. For example, the peak-to-peak variation is 0.15 mag at 2459 939.55 d in the top left panel, whereas it is 0.07 mag at 2459 939.57 d. Similar variations are also visible in the top right panel. Hence, there is clearly more than one frequency at play. Fourier transforms of each light curve shows that there are three significant frequencies detected, F1 at ≈390, F2 at ≈410, and the combination frequency F1 + F2 at ≈800 cycles per day. F2 is resolved better in the second night's data given its longer baseline. In addition, both F1 and F2 are detected above the 5⟨A⟩ level in both nights of Gemini observations. The amplitudes of the two modes appear to change from night to night, similar to what is seen in the APO data, and also similar to the ultramassive white dwarf GD 518 (Hermes et al. 2013).

Tables 2 and 3 present the results from the frequency analysis of the APO and Gemini data, respectively. We report the results from both a least-square analysis and a Monte Carlo approach where we replace each photometric measurement m with $m + g\ \delta m$, where δm is the error in magnitude and g is a Gaussian deviate with zero mean and unit variance. For each of the 1000 sets of modified light curves for each night, we calculate the Fourier transform using the PERIOD04 package in batch mode (Lenz & Breger 2014), and we take the range that encompasses 68 per cent of the probability distribution function as the 1σ uncertainties in frequency and amplitude. The results from the least-squares and the Monte Carlo analysis agree within the errors, but we adopt the results from the latter as it provides a better estimate of the error distribution.

The APO data reveal two dominant modes at $220.44^{+0.50}_{-0.42}$ and $211.18^{+0.63}_{-0.66}$ s with 32–35 mmag amplitudes, whereas the Gemini data show the same modes at $222.49^{+0.61}_{-0.57}$ and $206.47^{+0.88}_{-0.71}$ s on 2022 December 26, and $221.46^{+0.30}_{-0.31}$ and $209.52^{+0.66}_{-0.71}$ s on December 27. It is possible that the observed modes in J0049−2525 are unstable, and the observed frequency variations in the Gemini data are real. However, due to the relatively short baseline (47 min) of the observations on December 26, the dominant peak in the Fourier transform is relatively broad, and our measurements of the frequencies are likely impacted by the observing window. Hence, the frequency measurements from December 27 are superior, and they are also consistent with the APO data within 2σ.

Combining APO and Gemini results, the weighted mean frequencies are F1 = 221.36 ± 0.23 s and F2 = 209.38 ± 0.40 s. The observed multiperiodic variations in J0049−2525 over four different nights confirm it as the most massive pulsating white dwarf currently known. J0049−2525 is significantly more massive than the previous record holders BPM 37093 and GD 518. In addition, the latter objects show variations at the 1–4 mmag level (Metcalfe et al. 2004; Hermes et al. 2013), whereas J0049−2525 has pulsations at the 30 mmag level, making it much easier to detect its variability.

4 DISCUSSION

4.1 Asteroseismology of ultramassive white dwarfs

Ultramassive white dwarfs are expected to have a significant portion of their cores in a crystalline state at the effective temperatures near the ZZ Ceti instability strip. For J0049−2525, the crystallized fraction is expected to be $\gtrsim$99 per cent.

Table 3. Multimode frequency solutions based on the Gemini data.

Date	ID	Method	Frequency (cycles d^{-1})	Period (s)	Amplitude (mmag)
2022 Dec 26	F1	LSQ	388.34 ± 0.67	222.48 ± 0.38	41.9 ± 1.6
–	F2	LSQ	418.36 ± 1.20	206.52 ± 0.59	23.1 ± 1.6
–	F1 + F2	LSQ	796.06 ± 2.33	108.53 ± 0.32	12.0 ± 1.6
2022 Dec 27	F1	LSQ	390.22 ± 0.57	221.42 ± 0.32	27.7 ± 1.6
–	F2	LSQ	412.16 ± 1.09	209.63 ± 0.55	14.5 ± 1.6
–	F1 + F2	LSQ	802.02 ± 1.63	107.73 ± 0.22	9.6 ± 1.6
2022 Dec 26	F1	MC	$388.33^{+1.00}_{-1.05}$	$222.49^{+0.61}_{-0.57}$	$41.8^{+2.0}_{-1.7}$
–	F2	MC	$418.47^{+1.44}_{-1.78}$	$206.47^{+0.88}_{-0.71}$	$23.3^{+2.0}_{-1.7}$
–	F1 + F2	MC	$795.93^{+3.49}_{-4.55}$	$108.55^{+0.62}_{-0.47}$	$12.2^{+1.7}_{-1.6}$
2022 Dec 27	F1	MC	$390.13^{+0.55}_{-0.53}$	$221.46^{+0.30}_{-0.31}$	$27.9^{+1.4}_{-1.3}$
–	F2	MC	$412.38^{+1.41}_{-1.29}$	$209.52^{+0.66}_{-0.71}$	$14.9^{+1.5}_{-1.4}$
–	F1 + F2	MC	$801.26^{+1.88}_{-...}$	$107.83^{+...}_{-0.25}$	$10.2^{+1.1}_{-1.1}$

Asteroseismology can provide insight into the interior structure of ZZ Ceti white dwarfs, although periods (Π) and period spacings ($\Delta\Pi$) vary with mass, effective temperature, H envelope mass, and the crystallized mass fraction. In other words, there are four parameters to fit, but the crystallized mass fraction is also a function of the stellar mass and temperature and therefore is not independent. Crystallization (i) shrinks the resonant cavity, which results in a growth in the period spacing, additional to that due to cooling only, (ii) engulfs the entire region of the core, and these regions and their chemical compositions become impossible to probe with pulsations since the g modes cannot penetrate the crystallized matter. Due to crystallization, the mode trapping properties and the resulting period-spacing features are largely simplified because only the He/H transition remains active. The results of (i) and (ii) are a $\Delta\Pi$ distribution with much less features even for short periods (low order modes), and mean period spacing much higher than what would be without crystallization (see Montgomery et al. 1999; Córsico et al. 2005).

The fact that g-mode eigenfunctions cannot penetrate the solid regions of the core makes it virtually impossible to discriminate the deep core chemical composition (CO versus ONe) with pulsations in the most ultramassive DAV white dwarfs. However, for less massive ones, e.g. with $M_\star \sim 1.1$ M$_\odot$, features of the outermost parts of the core can be probed by means of pulsations, which may be enough to distinguish between CO and ONe cores (see figs 2 and 3 from De Gerónimo et al. 2019).

Córsico et al. (2019b) performed asteroseismological analysis of several pulsating ultramassive WDs, among them, BPM 37093, the richest pulsator known. Using the eight modes identified by Metcalfe et al. (2004), the authors were able to perform period spacing analysis and period-to-period fits. On the other hand, for GD 518, which exhibits just three modes (Hermes et al. 2013), only period-to-period fits were performed. For BPM 37093, the mean period spacing of ∼17 s corresponds to $\ell = 2$ g modes. Due to the degeneracy of the dependence of the mean period spacing on stellar mass, effective temperature, and the H envelope mass, Córsico et al. (2019b) could not independently infer the mass of the star, but they could restrict possible solutions by comparing the observed period spacing with the average theoretical period spacings. They found a best-fitting model by considering the individual pulsation periods. The best-fitting asteroseismological model for BPM 37093 has $T_{\rm eff} = 11\,650$ K, $M_\star = 1.16$ M$_\odot$, $\log(M_{\rm H}/M_\star) = -6$, and a crystallized mass fraction of 92 per cent.

The case of ultramassive DBVs, if they exist, would be more encouraging, because in this case, crystallization in the DBV instability strip ($T_{\rm eff} \sim 24\,000$–$30\,000$ K) is not capable of hiding the chemical composition of the core completely (Córsico et al. 2021).

4.2 Representative asteroseismological models for J0049−2525

With only two significant modes detected, it is impossible to perform a detailed asteroseismological analysis of J0049−2525. For instance, in order to put constraints on the mass of the H envelope, it is necessary to have many periods available in such a way that one can construct period-spacing diagrams ($\Delta\Pi$ versus Π). The quantity $\Delta\Pi$ is very sensitive to $M_{\rm H}$. In particular, thick H envelopes give rise to short trapping cycles (intervals between $\Delta\Pi$ minima) and low amplitudes of trapping (magnitude of $\Delta\Pi$ minima), while thin H envelopes result in long trapping cycles and very deep minima of $\Delta\Pi$ (Brassard et al. 1992). Because we cannot create a period-spacing diagram for J0049−2525 based on only two frequencies, we have to resort to the individual period fits to find representative seismological models.

We use an expanded grid of evolutionary sequences of ultramassive white dwarfs with ONe cores and stellar masses $M_\star = 1.10$, 1.13, 1.16, 1.19, 1.22, 1.25, 1.29 M$_\odot$ and H layer masses between 10^{-6} and $10^{-10} M_\star$ (De Gerónimo et al, in prepration). The evolutionary models were computed using the LPCODE (Althaus et al. 2005), taking into account Coulombian diffusion (Althaus, Córsico & De Gerónimo 2020). Further details are provided in Camisassa et al. (2019) and Córsico et al. (2019b). We computed adiabatic pulsation periods of $\ell = 1$, 2 g modes in the range 70–1500 s, as is typically observed in ZZ Ceti stars, employing the `LP-PUL` pulsation code (Córsico et al. 2019b). The asymptotic period spacing for ultramassive DA white dwarfs with masses between 1.10 and 1.29 M$_\odot$ and effective temperatures within the ZZ Ceti instability strip (13 500–10 500 K) varies between ∼22 s and ∼34 s for $\ell = 1$, and between ∼12 and ∼19 s for $\ell = 2$.

With only two periods observed in J0049−2525, there are many possible models that reproduce both periods at the same time. The two periods are relatively close to each other (209 and 221 s). We adopted different scenarios for the mode identification: (a) they are both $\ell = 1$ (or both $\ell = 2$) and consecutive modes, associated to a minimum in $\Delta\Pi$ due to mode trapping. This is unlikely, but can be checked by performing period-to-period fits assuming that both periods are $\ell = 1$ or 2; (b) one period is $\ell = 1$ and the other one is

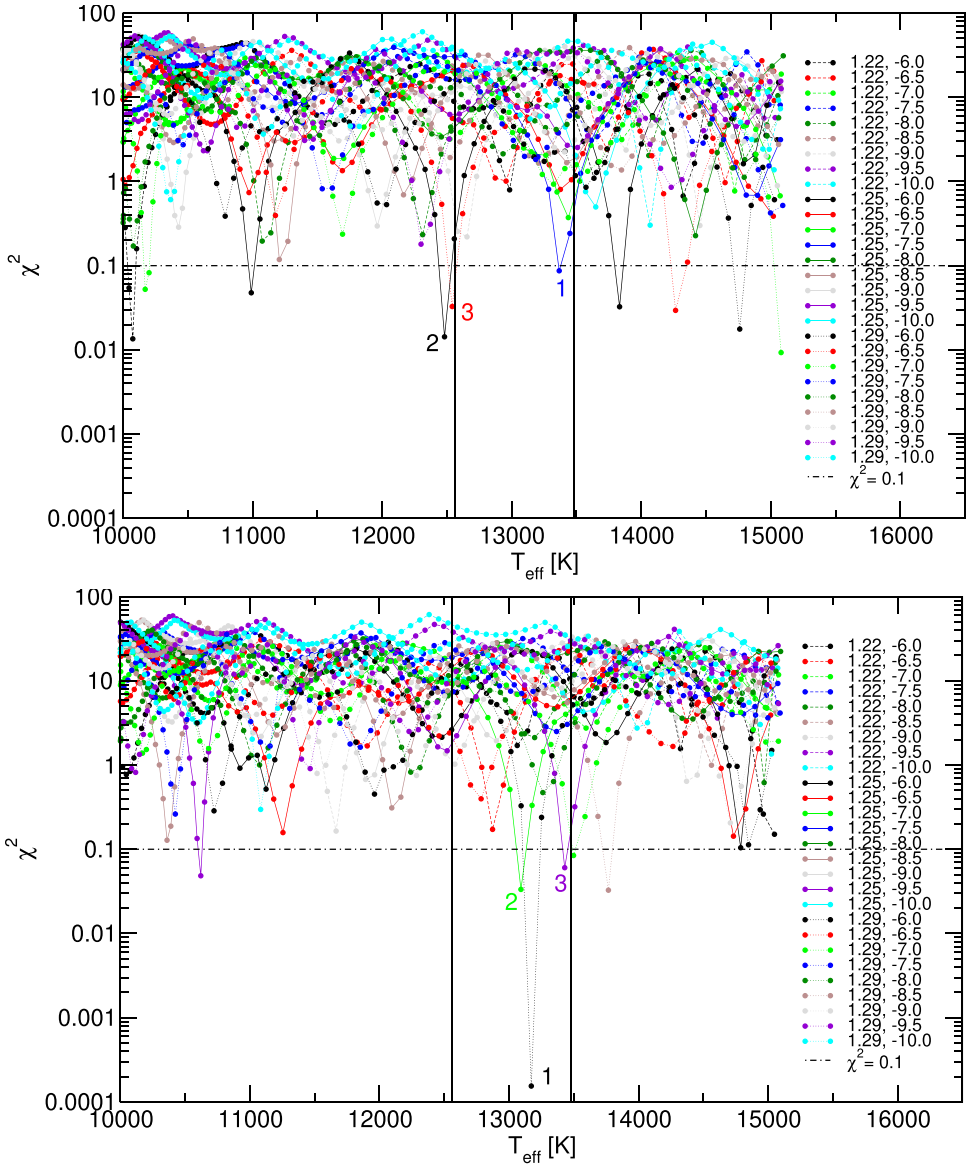

Figure 3. The χ^2 of the period fit as a function of the effective temperature for the ultramassive DA white dwarf model sequences with $M_\star = 1.22$ to $1.29\,M_\odot$ and H envelopes ranging from 10^{-6} to $10^{-10}\,M_\star$. Vertical solid lines show the $\pm1\sigma$ range of the spectroscopic effective temperature for J0049−2525. The top panel shows the fits to the weighted mean periods obtained from APO and Gemini data, whereas the bottom panel shows the fits using the periods measured only from the APO data. Three best-fitting models are labelled as 1, 2, and 3 in each panel, and their parameters are given in Table 4.

$\ell = 2$, which can also be checked in the period-to-period fits, leaving the mode identification as a free parameter; and a more unlikely option (c) it is a rotational triplet ($\ell = 1$) where one of the components does not appear for some reason. In this case, (i) the components would be $m = 0$ and $m = +1$ or $m = -1$ (one of the latter is missing), or (ii) the components would be $m = +1$ and $m = -1$, with the $m = 0$ component missing.

We carried out period fits considering (i) both periods as $\ell = 1$, (ii) both periods as $\ell = 2$, and (iii) one period is $\ell = 1$ and the other is $\ell = 2$, without initially setting the ℓ value for each period. We adopted the weighted mean periods of 209.4 and 221.4 s. To evaluate the agreement between the theoretical and observed periods, we used the expression:

$$\chi^2(M_\star, M_{\rm H}, T_{\rm eff}) = \frac{1}{N}\sum_{i=1}^{N} \min[(\Pi_i^{\rm O} - \Pi_k^{\rm th})^2], \qquad (1)$$

where N is the number of detected modes, $\Pi_i^{\rm O}$ are the observed period and $\Pi_k^{\rm th}$ are the periods computed theoretically (k is the radial order). The best-fitting model is selected by searching for the minimum value of χ^2. We did not consider the theoretical density of modes here, because this is a preliminary analysis (due to having only two periods) and also begcause we do not have a reliable recipe that takes into account the density of modes according to the harmonic degree and/or the stellar mass in a self-consistent way.

In general, we obtained poor solutions when both modes are $\ell = 1$ or $\ell = 2$, and we can rule out these possibilities. On the other hand, a mixture of $\ell = 1$ and $\ell = 2$ modes provide much better fits to the observed periods. Fig. 3 shows the quality function χ^2 as a function of the effective temperature of the star. Given the spectroscopic mass of the star ($1.26\,M_\odot$ for an ONe core), here we only display models with $M_\star \geq 1.22\,M_\odot$. For comparison, the top panel shows the fits to the weighted mean periods obtained from APO and Gemini data,

Table 4. Representative asteroseismic models for J0049−2525. The top (bottom) three lines correspond to the models labelled in the top (bottom) panel of Fig. 3.

Model	Mass ($M_\odot$)	log g (cm s^{-2})	$T_{\rm eff}$ (K)	log $\frac{M_{\rm H}}{M_\star}$	$\frac{M_{\rm crys}}{M_\star}$ (per cent)	d (pc)
1	1.25	9.274	13 367	−7.5	98.8	111.1 ± 1.7
2	1.25	9.271	12 482	−6.0	98.7	104.4 ± 1.6
3	1.29	9.419	12 541	−6.5	99.6	91.0 ± 1.4
1	1.29	9.414	13 172	−6.0	99.4	95.2 ± 1.5
2	1.25	9.276	13 092	−7.0	98.7	108.8 ± 1.7
3	1.25	9.278	13 430	−9.5	98.7	111.1 ± 1.7

whereas the bottom panel shows the fits using the periods measured only from the APO data. In each case, there are many possible solutions with $\chi^2 < 0.1$, but there are a few that fall within or near the 1σ range of the spectroscopic effective temperature of J0049−2525. We present the parameters of the three best-fitting models in each case in Table 4. These models indicate a crystallized mass fraction of 98.7–99.6 per cent.

A slight shift in the periods used in the model fits leads to very different results. The extreme sensitivity of the results to the precise values of the periods used is due to the fact that there are only two periods observed. For example, we find an excellent fit to the periods derived from the APO data only with a model that has $M_\star = 1.29\,{\rm M}_\odot$, $T_{\rm eff} = 13\,172$ K, and $M_{\rm H} = 10^{-6}\,M_\star$. This is the model labelled as 1 in the bottom panel of Fig. 3. The seismological distance of this model, 95.2 ± 1.5 pc, is also consistent with the *Gaia* distance of $99.7^{+2.9}_{-2.7}$ pc (Bailer-Jones et al. 2021) within the errors. Even though this is an excellent representative model of the star, we caution that there are many other possible solutions, and we have to wait for the detection of additional periods in this object to provide a more robust seismological solution.

5 CONCLUSIONS

We report the discovery of multiperiodic variability in J0049−2525, a ∼1.3 $M_\odot$ ultramassive white dwarf within the 100 pc sample. J0049−2525 does not display any of the signatures of binary mergers; there is no evidence of magnetism, rapid rotation, or large tangential velocity ($V_{\rm tan} = 17$ km s^{-1}). Its spectrum is that of a typical DA white dwarf. Assuming that it formed through single star evolution, it is likely to have an ONe core. The best-fitting model to its observed spectral energy distribution places it within the boundaries of the ZZ Ceti instability strip.

We detected ∼30 mmag variations in J0049−2525 at two different frequencies over four different nights, confirming it as the most massive pulsating DAV white dwarf currently known. Fig. 4 shows the masses and effective temperatures for the ZZ Ceti white dwarfs in the 100 pc white dwarf sample from Vincent et al. (2020) assuming CO cores. Ultramassive ZZ Ceti white dwarfs with $M_\star > 1\,{\rm M}_\odot$ are labelled. Note that two of these objects, J0551+4135 and J0204+8713, lack follow-up optical spectroscopy. Hence, their classification as DAV white dwarfs requires confirmation. Another candidate that also needs follow-up spectroscopy for confirmation, J212402.03−600100.0, was too far south to be included in the Vincent et al. (2020) study, and therefore not shown here.

J0049−2525 is significantly more massive than the other pulsating DAV white dwarfs known. Its mass is 1.312 ± 0.010 or 1.263 ± 0.011 for a CO or ONe core, respectively (Kilic et al. 2023). Evolutionary

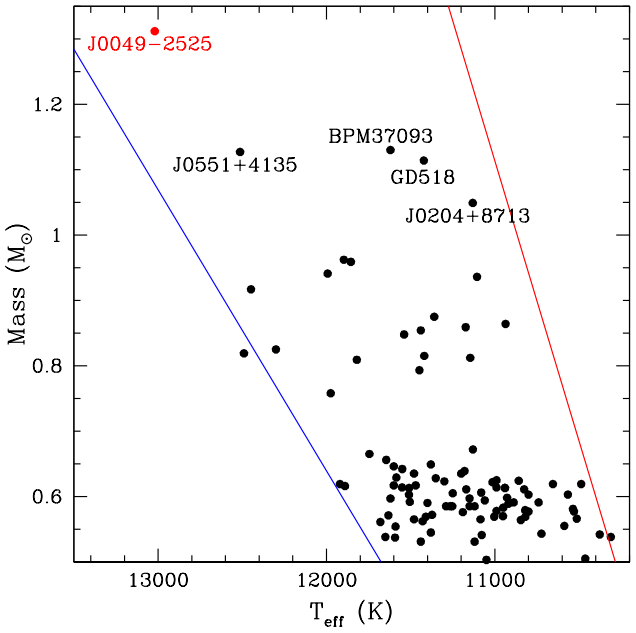

Figure 4. Masses and effective temperatures for the previously known ZZ Ceti white dwarfs in the 100 pc white dwarf sample from Vincent et al. (2020) assuming CO cores. The blue and red lines show the empirical boundaries of the instability strip from the same work. Ultramassive ZZ Ceti white dwarfs with $M > 1\,{\rm M}_\odot$ are labelled.

models predict that its interior is $\gtrsim$ 99 per cent crystallized. Asteroseismology offers a unique opportunity to probe the interior structure of crystallized massive white dwarfs like J0049−2525, provided that a sufficient number of g modes with consecutive radial order are detected. Because periods and their spacings vary with mass, effective temperature, H envelope mass, and the crystallized mass fraction, and because J0049−2525 displays only two significant modes in our APO and Gemini data, it is impossible to find a unique seismic solution. We provide several representative solutions that can match the observed characteristics of this star. However, a significant number of additional pulsation modes would need to be detected to overcome the degeneracies in the asteroseismic fits. We encourage extensive follow-up time-series photometry campaigns on this unique target.

ACKNOWLEDGEMENTS

This work is supported in part by the National Science Foundation under grants AST-1906379 and AST-2205736, the National Aeronautics and Space Administration under grant no. 80NSSC22K0479, by AGENCIA through the Programa de Modernización Tecnológica BID 1728/OC-AR, and by the PIP 112-200801-00940 grant from CONICET. FCDG acknowledges financial support provided by ANID-FONDECYT grant no. 3200628.

The Apache Point Observatory 3.5 m telescope is owned and operated by the Astrophysical Research Consortium.

Based on observations obtained at the international Gemini Observatory, a programme of NSF's NOIRLab, which is managed by the Association of Universities for Research in Astronomy (AURA) under a cooperative agreement with the National Science Foundation on behalf of the Gemini Observatory partnership: the National Science Foundation (United States), National Research Council (Canada), Agencia Nacional de Investigación y Desarrollo (Chile), Ministerio

de Ciencia, Tecnología e Innovación (Argentina), Ministério da Ciência, Tecnologia, Inovações e Comunicações (Brazil), and Korea Astronomy and Space Science Institute (Republic of Korea).

DATA AVAILABILITY

The data underlying this article are available in the Gemini Observatory Archive at https://archive.gemini.edu, and can be accessed with the programme number GS-2022B-DD-107. The APO data that support the findings of this study are available from the corresponding author upon reasonable request.

REFERENCES

Althaus L. G., Serenelli A. M., Panei J. A., Córsico A. H., García-Berro E., Scóccola C. G., 2005, A&A, 435, 631
Althaus L. G., Córsico A. H., De Gerónimo F., 2020, A&A, 644, A55
Althaus L. G. et al., 2021, A&A, 646, A30
Bailer-Jones C. A. L., Rybizki J., Fouesneau M., Demleitner M., Andrae R., 2021, AJ, 161, 147
Bé dard A., Bergeron P., Fontaine G., 2017, ApJ, 848, 11
Brassard P., Fontaine G., Wesemael F., Hansen C. J., 1992, ApJS, 80, 369
Caiazzo I. et al., 2021, Nature, 595, 39
Camisassa M. E. et al., 2019, A&A, 625, A87
Córsico A. H., Althaus L. G., Montgomery M. H., García-Berro E., Isern J., 2005, A&A, 429, 277
Córsico A. H., Althaus L. G., Miller Bertolami M. M., Kepler S. O., 2019a, A&A Rev., 27, 7
Córsico A. H., De Gerónimo F. C., Camisassa M. E., Althaus L. G., 2019b, A&A, 632, A119
Córsico A. H., Althaus L. G., Gil-Pons P., Torres S., 2021, A&A, 646, A60
Curd B., Gianninas A., Bell K. J., Kilic M., Romero A. D., Allende Prieto C., Winget D. E., Winget K. I., 2017, MNRAS, 468, 239
De Gerónimo F. C., Córsico A. H., Althaus L. G., Wachlin F. C., Camisassa M. E., 2019, A&A, 621, A100
Dufour P., Blouin S., Coutu S., Fortin-Archambault M., Thibeault C., Bergeron P., Fontaine G., 2017, in Tremblay P. E., Gaensicke B., Marsh T., eds, ASP Conf. Ser. Vol. 509, 20th European White Dwarf Workshop, The Montreal White Dwarf Database: a Tool for the Community. ASP, San Francisco, p. 3
Fontaine G., Brassard P., 2008, PASP, 120, 1043
Fontaine G., Brassard P., Bergeron P., 2001, PASP, 113, 409
Giammichele N. et al., 2018, Nature, 554, 73
Gianninas A., Bergeron P., Ruiz M. T., 2011, ApJ, 743, 138
Hermes J. J., Kepler S. O., Castanheira B. G., Gianninas A., Winget D. E., Montgomery M. H., Brown W. R., Harrold S. T., 2013, ApJ, 771, L2
Kanaan A., Kepler S. O., Giovannini O., Diaz M., 1992, ApJ, 390, L89
Kepler S. O., Koester D., Ourique G., 2016, Science, 352, 67
Kilic M., Bergeron P., Kosakowski A., Brown W. R., Agüeros M. A., Blouin S., 2020, ApJ, 898, 84
Kilic M., Bergeron P., Blouin S., Bédard A., 2021a, MNRAS, 503, 5397
Kilic M., Kosakowski A., Moss A. G., Bergeron P., Conly A. A., 2021b, ApJ, 923, L6
Kilic M. et al., 2023, MNRAS, 518, 2341
Lenz P., Breger M., 2014, Astrophysics Source Code Library, record ascl:1407.009
Metcalfe T. S., Montgomery M. H., Kanaan A., 2004, ApJ, 605, L133
Montgomery M. H., Klumpe E. W., Winget D. E., Wood M. A., 1999, ApJ, 525, 482
Mukadam A. S., Owen R., Mannery E., MacDonald N., Williams B., Stauffer F., Miller C., 2011, PASP, 123, 1423
Murai T., Sugimoto D., Hōshi R., Hayashi C., 1968, Prog. Theor. Phys., 39, 619
Pshirkov M. S. et al., 2020, MNRAS, 499, L21
Rowan D. M., Tucker M. A., Shappee B. J., Hermes J. J., 2019, MNRAS, 486, 4574
Schwab J., 2021, ApJ, 906, 53
Vincent O., Bergeron P., Lafrenière D., 2020, AJ, 160, 252
Winget D. E., Kepler S. O., 2008, ARA&A, 46, 157

This paper has been typeset from a TEX/LATEX file prepared by the author.